

Interactions of 4.09-GeV/ c positive pions with protons: $\pi^+p \rightarrow$ four charged particles plus neutrals*

D. G. Fong, J. T. Massimo, S. Pitluck,[†] A. M. Shapiro, R. L. Simard, and M. Widgoff

Department of Physics, Brown University, Providence, Rhode Island 02912

(Received 19 February 1974)

The reactions of positive pions with protons yielding four charged particles and one or more neutrals have been studied, especially the reaction $\pi^+p \rightarrow \Delta^{++}\omega^0 \rightarrow p\pi^+\pi^+\pi^-\pi^0$. The results presented in this paper were obtained from a 100 000-picture exposure of the Argonne-MURA 30-in. liquid hydrogen bubble chamber, with a beam of incident pions of 4.09-GeV/ c momentum. Comparisons have been made with corresponding results of other experiments at various incident beam momenta, and with the predictions of some theoretical models of the π^+p interaction.

I. INTRODUCTION

The results presented in this paper were obtained from a 100 000-picture exposure of the Argonne-MURA 30-in. liquid hydrogen bubble chamber at the Argonne National Laboratory.¹ The incident beam of π^+ mesons had a momentum of 4.09 GeV/ c at the center of the bubble chamber. Cross sections for various interactions are given, as well as a detailed description of the exclusive reaction $\pi^+p \rightarrow \Delta^{++}\omega^0 \rightarrow p\pi^+\pi^+\pi^-\pi^0$. Comparisons have been made with corresponding results from other studies at various momenta.²

II. CROSS SECTIONS

The film was scanned for all interactions of the beam particles. Approximately one-half the events were measured with the MIT PEPR (Precision Encoding and Pattern Recognition) system after pre-digitizing at Brown; the remainder, including events which were judged unsuitable for PEPR and those which PEPR failed to measure, were hand measured. Reconstruction of the events in space and kinematic fitting were carried out by means of the programs TVGP and SQUAW. The ionization density of each track was determined by PEPR for the automatically measured events, and was visually estimated for each hand-measured event. Each kinematic hypothesis found successful by SQUAW was required also to be consistent with the ionization information.

In order to ensure accuracy in the measurements, the final sample was limited to events with their interaction points in a fiducial volume which provided that the incoming track had a measurable length of at least 17 cm, and each outgoing track a measurable length of at least 21 cm in the chamber. The predetermined beam momentum of 4.09 ± 0.10 GeV/ c was used in SQUAW, with the measured direction of the incoming particle for each

event.

The total number of events of all topologies found within the fiducial volume was 21 448. This number was corrected for scanning efficiency, determined as a function of topology by double scanning about 10% of the film. The efficiencies were $(95 \pm 1)\%$ for two-prong, $(97 \pm 1)\%$ for four-prong, $(98 \pm 1)\%$ for six-prong, and $(99 \pm 1)\%$ for eight-prong events. An additional correction was made for elastic scattering events in which the pion was deflected through angles less than 2° , as such events tend to be systematically missed by the scanners and are therefore not taken into account by the double-scanning efficiency correction. The corrected total number of events occurring in the fiducial volume was calculated to be 23 158.³ With the total π^+p cross section at 4.09 GeV/ c taken to be equal to 27.62 ± 0.03 mb, from the counter experiment of Citron *et al.*,⁴ this number of events corresponds to a cross section of $1.193 \mu\text{b}$ per event (corrected) in this experiment. The cross sections for all charged-particle multiplicities are given in Table I. The inclusive reactions $\pi^+p \rightarrow \pi^+X$ and $\pi^+p \rightarrow \pi^-X$ have been studied for this entire group of events, and the results have been given in another paper.⁵ In this paper we will discuss events with four charged particles and one known neutral particle in the final state—events which are fitted by SQUAW with one constraint (1C). In particular, we will consider in detail events produced via the interaction

$$\pi^+p \rightarrow p\pi^+\pi^+\pi^-\pi^0 \quad (1C). \quad (1)$$

Only cross-section information will be given for the reaction

$$\pi^+p \rightarrow n\pi^+\pi^+\pi^-\pi^0 \quad (1C). \quad (2)$$

Among the four-prong events, in addition to (1) and (2), the following final states were identified:

TABLE I. Cross sections for production of events with two to eight charged particles.

Topology	Events measured	Small-angle scatter loss	Scan efficiency	Total events	Cross section (mb)
2-prong	12 910	734	0.95 ± 0.01	14 362	17.13 ± 0.24
4-prong	7913	...	0.97 ± 0.01	8158	9.73 ± 0.15
6-prong	617	...	0.98 ± 0.01	630	0.75 ± 0.03
8-prong	8	...	0.99 ± 0.01	8	0.01 ± 0.003
Totals	21 448	734		23 158	27.62

$$\pi^+p \rightarrow p\pi^+\pi^+\pi^- \quad (4C), \quad (3)$$

$$\pi^+p \rightarrow p\pi^+\pi^+\pi^-MM \quad (0C), \quad (4)$$

and

$$\pi^+p \rightarrow \pi^+\pi^+\pi^+\pi^-MM \quad (0C). \quad (5)$$

Reaction (3) gives a four-constraint (4C) fit; if an event had both 4C and 1C fits, the 4C fit was chosen. Also, a successful 1C fit was chosen in preference to an acceptable 0C fit.

Before abandoning a 4C fit for a 1C fit, or any constrained fit for a 0C fit, on the basis of ionization inconsistencies alone, the ionization estimates were rechecked visually. Similarly, events which had more than one successful hypothesis at the same constraint level (4C or 1C) were checked to see if these ambiguities in identification could be resolved by ionization information. The numbers of unambiguously identified events of each of the reactions (1)–(5) are given in Table II. Events remaining with unresolved ambiguities amounted to just over 1% for 1C events [reactions (1) and (2)], and less than 0.5% for 4C events [reaction (3)]. There was a much larger number of ambiguities for 0C events, partly because of a lack of a further check of ionizations such as was made for 4C and 1C events.

The total number of four-prong events (Table I)

includes strange-particle production; however, no attempt has been made to fit strange-particle production hypotheses to these events. On the basis of a measured cross section of⁶ 0.424 ± 0.055 mb for the production of strange particles in four-prong interactions of pions of 4.0-GeV/*c* momentum, we estimate that about 345 such events were produced in the fiducial volume of this experiment. This number is consistent with the number of V^0 s and charged decays observed, and accounts for a large proportion of the 418 unidentified events mentioned in Table II.

In order to obtain the cross sections given in Table III for reactions (1)–(5), the ambiguous events and the unidentified events unaccounted for by strange-particle production were divided among the various reactions in proportions determined by the unambiguously identified events. Such uncertainly identified events amounted to less than about 2% of the total for each reaction except those including missing masses, reactions (4) and (5). As can be seen in Table III, the cross sections obtained in this experiment are in good agreement with cross sections measured in other experiments at nearby momenta. It should be noted that in calculating the cross sections given here, misidentification of events among the reactions has been assumed to be negligible.

TABLE II. Numbers of unambiguously identified events of reactions (1)–(5).

Reaction	Number of constraints	Number of events observed ^{a,b}
(1) $\pi^+p \rightarrow p\pi^+\pi^+\pi^-\pi^0$	1	2936
(2) $\pi^+p \rightarrow n\pi^+\pi^+\pi^-\pi^-$	1	727
(3) $\pi^+p \rightarrow p\pi^+\pi^+\pi^-$	4	2239
(4) $\pi^+p \rightarrow p\pi^+\pi^+\pi^-MM$	0	725
(5) $\pi^+p \rightarrow \pi^+\pi^+\pi^+\pi^-MM$	0	408
Total		7035

^a In addition to the 7035 unambiguously identified events listed above, there were 460 ambiguous events which satisfied more than one hypothesis at a given constraint level, as follows: 5 four-constraint, 45 one-constraint, and 410 zero-constraint fits. There were also 418 unidentified events, making a total of 7913 four-prong interactions seen.

^b The numbers in this table have not been corrected for the scanning efficiency. For four-prong events, this was (97 ± 1)%.

TABLE III. Cross sections for reactions (1)–(5).

Reaction	Cross section at $p_{lab}=4.09$ GeV/c (this experiment) ^a (mb)	Other experiments at nearby momenta	
		Cross section (mb)	Momentum p_{lab} (GeV/c)
(1) $\pi^+p \rightarrow p\pi^+\pi^+\pi^-\pi^0$	3.70 ± 0.08	3.41 ± 0.19 3.43 ± 0.69 3.78 ± 0.36	3.90^b 4.00^c 4.08^d
(2) $\pi^+p \rightarrow n\pi^+\pi^+\pi^-\pi^0$	0.91 ± 0.04	0.93 ± 0.19 0.97 ± 0.10	4.00^c 4.08^d
(3) $\pi^+p \rightarrow p\pi^+\pi^+\pi^0$	2.79 ± 0.07	3.09 ± 0.64 2.83 ± 0.21	4.00^c 4.08^d
(4) $\pi^+p \rightarrow p\pi^+\pi^+\pi^-\pi^0$	1.23 ± 0.05	1.33 ± 0.25	4.0^c
(5) $\pi^+p \rightarrow \pi^+\pi^+\pi^+\pi^-\pi^0$	0.68 ± 0.03	0.87	4.0^c
Total four-prong, nonstrange-particle production	9.31 ± 0.10	9.65	4.0^c
Total four-prong	9.73 ± 0.15		

^a Ambiguous and unidentified nonstrange-particle events have been divided statistically among reactions (1)–(5), in accordance with the proportions of unambiguously identified events. The errors are statistical only, based on numbers of identified events and the error in the efficiency measurements, and do not include an estimate of systematic errors in identification.

^b Pless *et al.*, Ref. 2.

^c M. Aderholz *et al.*, Phys. Rev. **138**, B897 (1965).

^d Brown *et al.*, Ref. 2.

The events which were unambiguously identified as proceeding via reaction (1) constitute the sample to be discussed in detail in the following sections.

III. THE REACTION $\pi^+p \rightarrow p\pi^+\pi^+\pi^-\pi^0$

Various two-, three-, and four-body effective mass plots for reaction (1) are shown in Figs. 1–6. The following mass limits for the various resonances were used in making the data cuts for all figures:

$$\Delta: 1116 < M(p\pi^+) < 1356 \text{ MeV}/c^2,$$

$$\omega: 733 < M(\pi^+\pi^-\pi^0) < 833 \text{ MeV}/c^2,$$

$$\eta: 508 < M(\pi^+\pi^-\pi^0) < 588 \text{ MeV}/c^2,$$

$$\rho: 640 < M(\pi\pi) < 890 \text{ MeV}/c^2.$$

A. Baryon resonances

Figure 1(a) shows the effective-mass distribution of the $p\pi^+$ combinations. The unshaded histogram shows two combinations for each event; the shaded histogram excludes $p\pi^+$ combinations for which

the π^+ is included in an ω^0 or η^0 resonance; the solid histogram is further restricted to combinations in which the momentum transfer to the $p\pi$ system is small: $|t| < 0.6$ (GeV/c)². The first two histograms, which include events of all $|t|$, show a substantial $\Delta^{++}(1236)$ signal on a large background, while in the histogram of events of low $|t|$, for $\Delta^{++}(1236)$ produced peripherally, the signal-to-background ratio is greatly enhanced.

Figures 1 and 7 [a scatter plot of effective masses $M(p\pi^+)$ vs $M(\pi^+\pi^-\pi^0)$] show that the $\Delta^{++}(1236)$ is produced via the interactions

$$\pi^+p \rightarrow \Delta^{++}\omega^0, \quad (6)$$

and

$$\pi^+p \rightarrow \Delta^{++}\eta^0, \quad (7)$$

as well as

$$\pi^+p \rightarrow \Delta^{++}\pi^+\pi^-\pi^0. \quad (8)$$

There is evidence also of $\pi^+p \rightarrow \Delta^{++}\rho\pi$ and $\pi^+p \rightarrow \Delta^{++}A_{1,2}$, seen against a large background (Figs. 3, 4, and 5).

The $p\pi^-$ and $p\pi^0$ effective-mass plots in Figs.

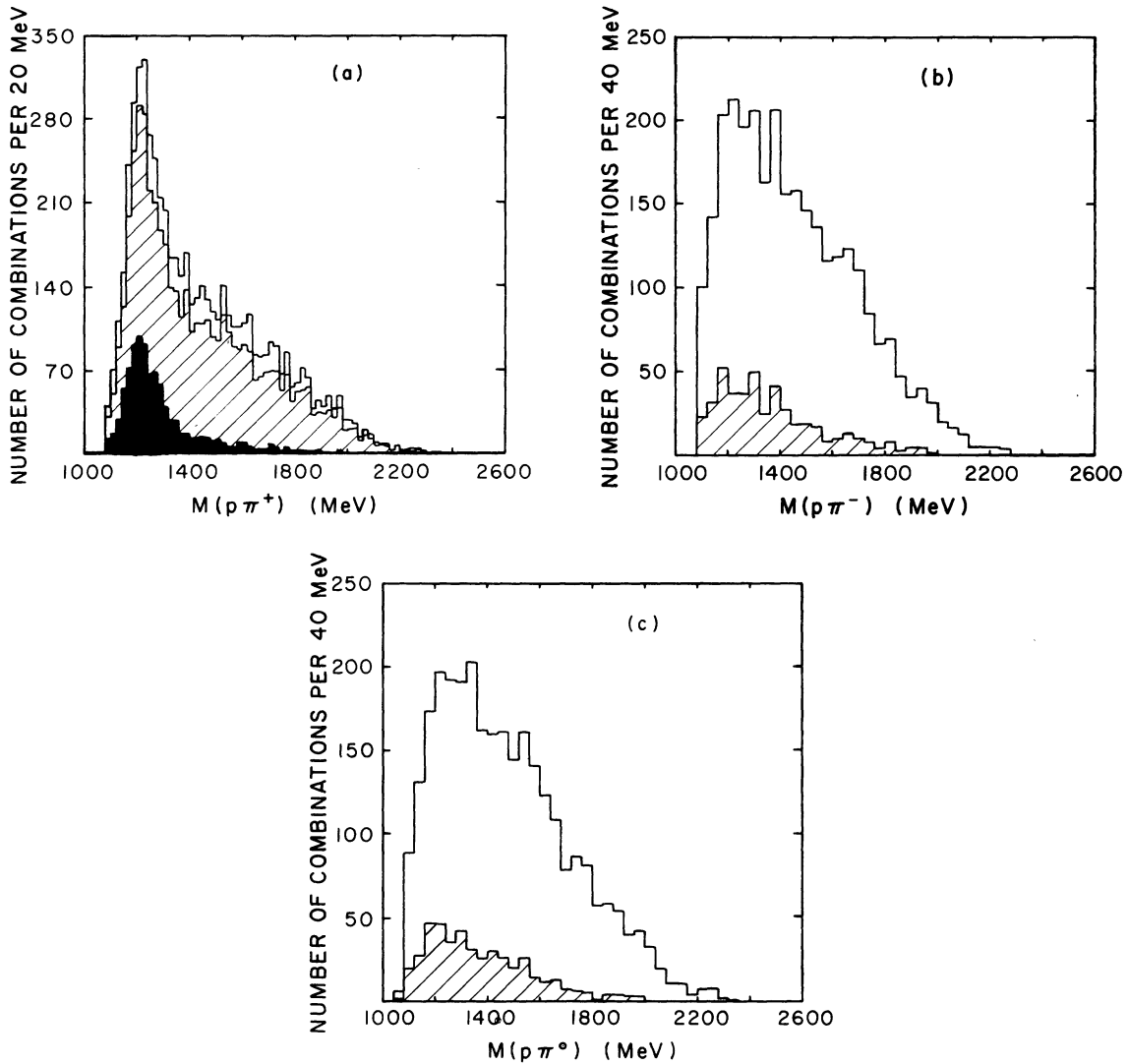


FIG. 1. (a) Distributions in $M(p\pi^+)$, the effective mass of $p\pi^+$ combinations produced in reaction (1). The clear histogram contains all the $p\pi^+$ combinations, two per event; the shaded histogram contains only those $p\pi^+$ pairings for which the π^+ is not included in an ω^0 or η^0 resonance; the solid histogram is restricted to those $p\pi^+$ combinations for which π^+ is not shared with an ω^0 or η^0 and the momentum transfer to the $p\pi^+$ system is small, $|t| < 0.6$ (GeV/c)². (b) Distributions in $M(p\pi^-)$, the effective mass of $p\pi^-$ produced in reaction (1). (c) Distributions in $M(p\pi^0)$, the effective mass of $p\pi^0$ produced in reaction (1). In (b) and (c) the clear histograms contain all the combinations, one per event, while the shaded histograms include only those for which the proton is not included in a $\Delta^{++}(1236)$ and the π^- or π^0 is not included in an ω^0 or η^0 resonance.

1(b) and 1(c), respectively, show that Δ^0 and Δ^+ production are both small, not readily distinguishable above the background. In Fig. 1(b) the clear histogram shows all the $p\pi^-$ combinations (one per event); the shaded histogram shows only those events for which the proton does not fit a $\Delta^{++}(1236)$ and for which the π^- meson does not fit an ω or η combination; Fig. 1(c) gives the corresponding histograms for the $p\pi^0$ combinations. Clearly, these requirements exclude a large percentage of

$p\pi^-$ and $p\pi^0$ combinations, leaving only a total of 451 among 2936 events. If one adds the requirement that the $p\pi^-$ or $p\pi^0$ combination should have a momentum transfer $|t| < 0.6$ (GeV/c)² (histograms not shown), all but a handful of events are eliminated, with 71 $p\pi^-$ and 75 $p\pi^0$ combinations remaining.

Mass distributions have been plotted for various combinations of the proton with two pions. These distributions for the most part are smooth and

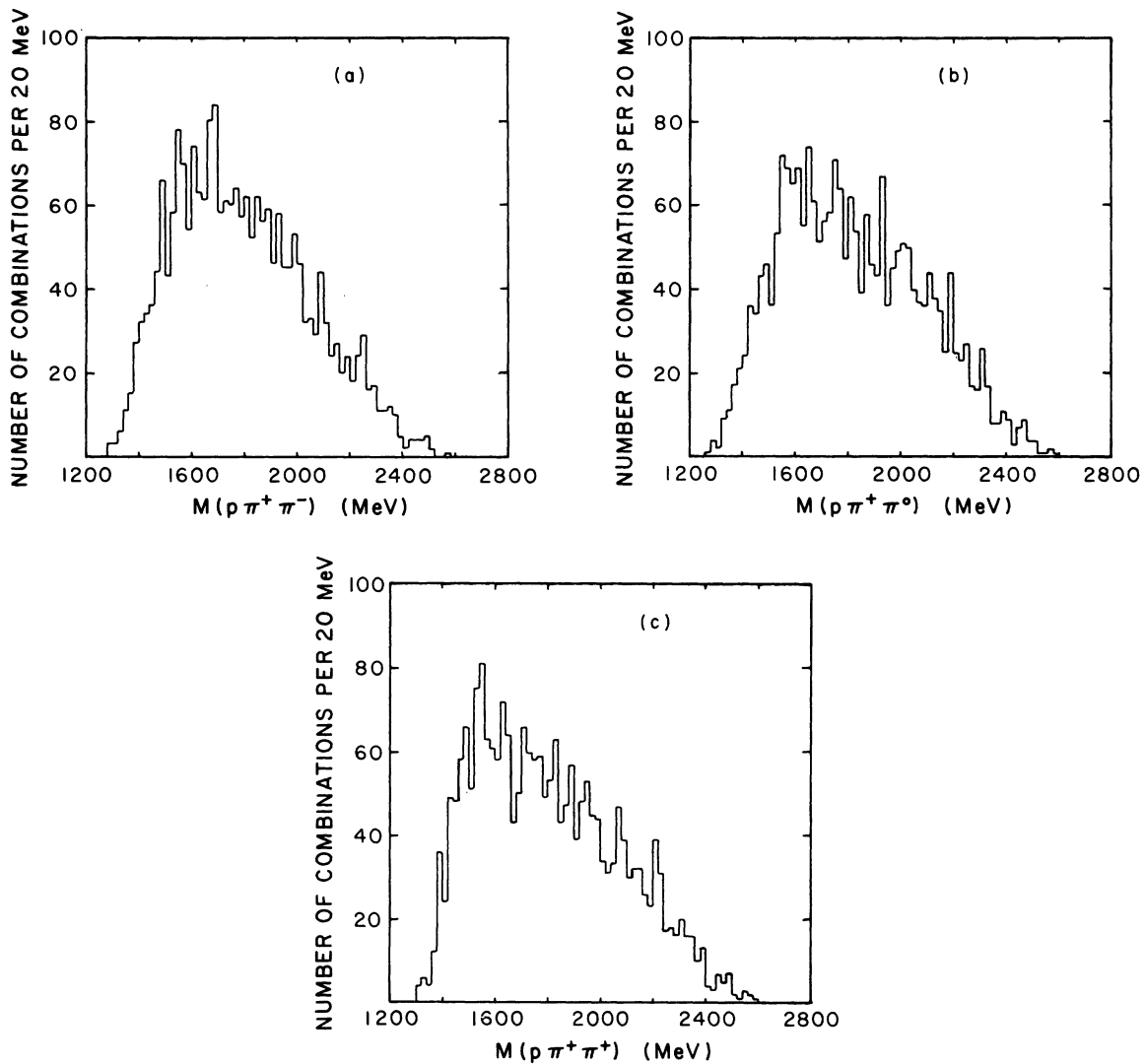


FIG. 2. Distributions in the effective masses of some proton and two-pion combinations from reaction (1): (a) $M(p\pi^+\pi^-)$, (b) $M(p\pi^+\pi^0)$, (c) $M(p\pi^+\pi^+)$. In each case a $p\pi\pi$ combination has been plotted only if $p\pi^+$ lies in the Δ^{++} band, and there is no ω^0 or η^0 .

show no distinguishable signs of resonance structure. In Fig. 2 are shown the $M(p\pi^+\pi^-)$, $M(p\pi^+\pi^0)$, and $M(p\pi^+\pi^+)$ plots, with $M(p\pi^+)$ in each case required to be in the $\Delta^{++}(1236)$ band, and with those combinations excluded for which the pions fit an ω^0 or an η^0 . The roughly triangular shape of the distributions, each rising steeply to a peak just below 1580 MeV/ c^2 , arises from the requirement that $1116 \leq M(p\pi^+) \leq 1356$ MeV/ c^2 . The $M(p\pi^+\pi^-)$ distribution, as compared with the doubly charged $M(p\pi^+\pi^0)$ and the triply charged $M(p\pi^+\pi^+)$, shows a possible enhancement in the region 1600–1720 MeV/ c^2 , which would be consistent with a signal from $N'(1670)$ and $N'(1688)$, both of which have isotopic spin $\frac{1}{2}$ and decay via $\Delta\pi$.

B. Meson resonances

Figure 3 shows the distributions of all the dipion mass combinations for reaction (1). In Figs. 3(a)–3(d) the unshaded histogram in each case shows all the possible two-pion combinations of the indicated charge; the shaded histograms exclude the combinations for which the pions fit an ω^0 or η^0 resonance, or, in the case of $\pi^+\pi^0$, an ω^0 , η^0 , or $\Delta^{++}(1236)$ resonance. Figure 3(d) shows the featureless $M(\pi^+\pi^+)$ distribution, for comparison. In Figs. 3(e)–3(g), the $\pi^+\pi^-$, $\pi^+\pi^0$, and $\pi^-\pi^0$ combinations are shown as in the shaded histograms of Figs. 3(a)–3(c), with the added condition that the dipion is accompanied by a $\Delta^{++}(1236)$. There

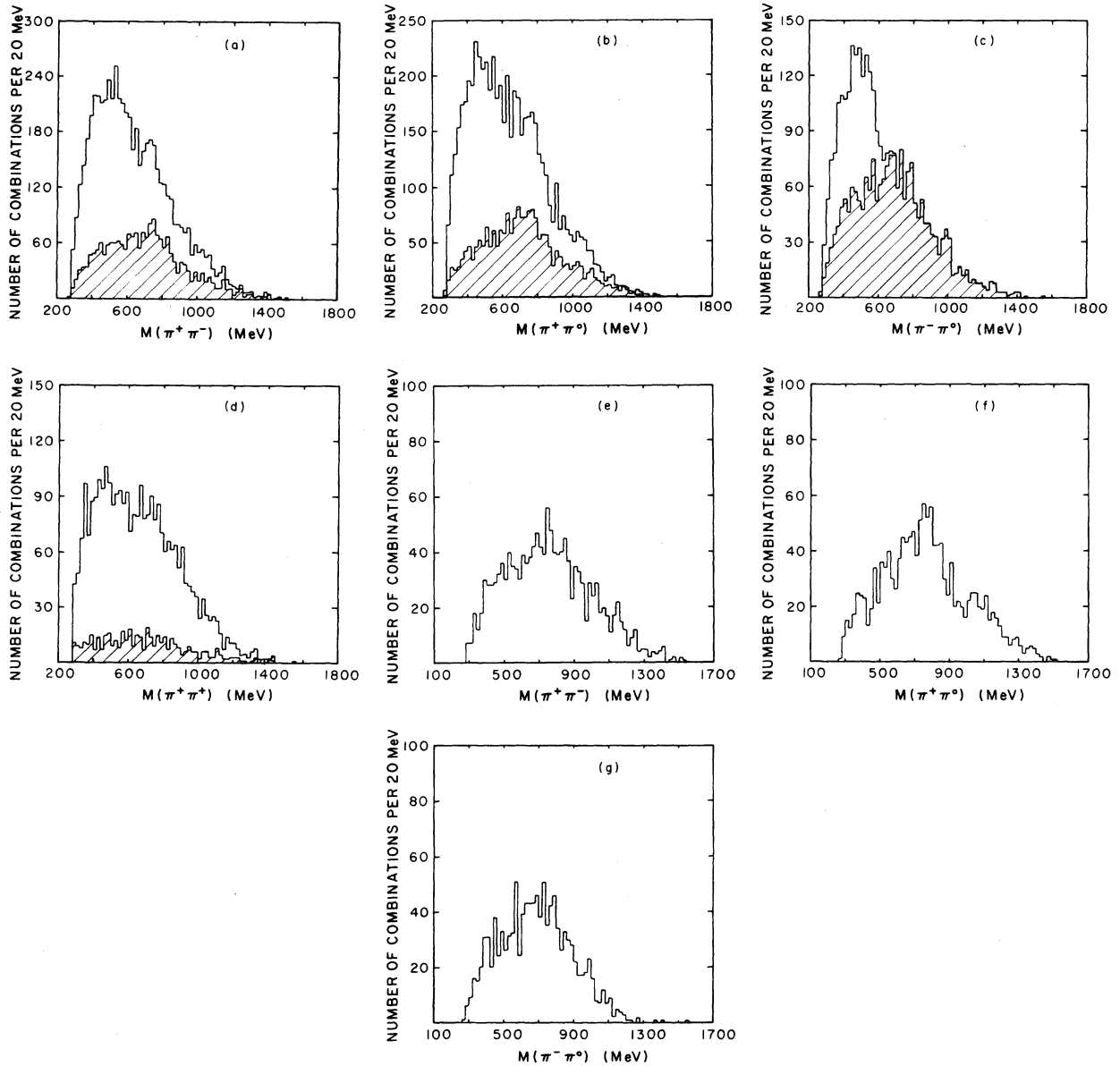


FIG. 3. (a)–(d) Distributions in the effective masses of various dipion combinations from reaction (1). (a) $M(\pi^+\pi^-)$, (b) $M(\pi^+\pi^0)$, (c) $M(\pi^-\pi^0)$, (d) $M(\pi^+\pi^+)$. In each of (a)–(d), the clear histogram shows all the combinations of the given charge for each event; the shaded histogram excludes any combinations in which one or both of the pions is included in a $\Delta^{++}(1236)$, ω^0 or η^0 resonance. (e)–(g) $M(\pi^+\pi^-)$, $M(\pi^+\pi^0)$, $M(\pi^-\pi^0)$, respectively, with the dipion required to be accompanied by $\Delta^{++}(1236)$, and with the further requirement that neither particle in the dipion combination is included in a $\Delta^{++}(1236)$, ω^0 , or η^0 resonance.

is a large background, against which charged and neutral ρ production are seen, both with and without an accompanying $\Delta^{++}(1236)$. Figure 3(f) shows a particular enhancement of the ρ^+ signal in the interaction $\pi^+p \rightarrow \Delta^{++}\rho^+\pi^-$.

Figure 4 shows the $\pi^+\pi^-\pi^0$ effective-mass distributions. The unshaded histogram includes two

combinations for each event, and both η^0 and ω^0 are clearly evident. The shaded histogram includes only those combinations $\pi_a^+\pi^-\pi^0$ that are accompanied by $\Delta^{++} \rightarrow p\pi_b^+$. About one-half of the ω^0 and over 40% of the η^0 are apparently produced with a Δ^{++} , via intermediate reactions (6) and (7). (See also Fig. 7.) Reaction (6) accounts for ap-

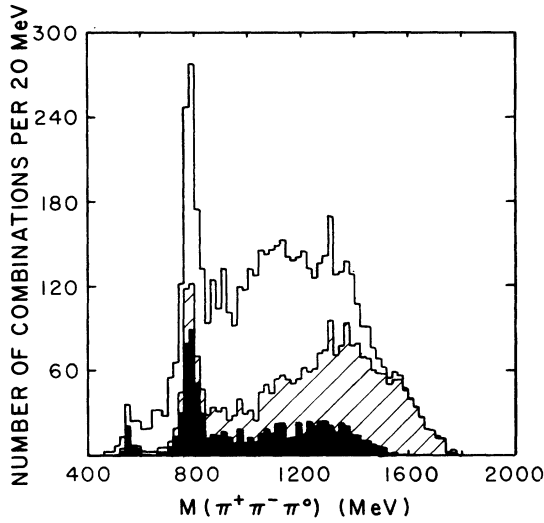


FIG. 4. Distributions in $M(\pi^+\pi^-\pi^0)$, the effective mass of $\pi^+\pi^-\pi^0$ combinations produced in reaction (1). The clear histogram includes all the combinations, two per event; the shaded histogram only those combinations $\pi_a^+\pi^-\pi^0$ which are produced with $\Delta^{++} \rightarrow p\pi_b^+$; the solid histogram is further limited to events with small momentum transfer to the $p\pi^+$ system, $|t| < 0.6$ (GeV/c)².

proximately 10% of interaction (1), and reaction (7) for just over 1%. Cross sections for these reactions, with corrections for background and efficiency, are given in Table IV. The signal-to-noise

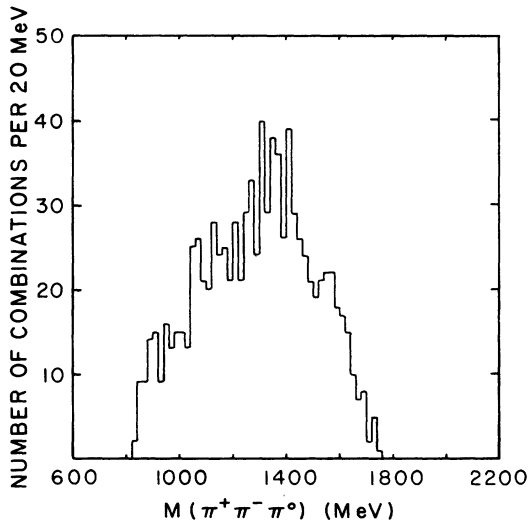


FIG. 5. Distribution in effective mass $M(\pi^+\pi^-\pi^0)$ from reaction (1), including only those tripton combinations that satisfy the following requirements: The effective mass of a combination of two of the pions of the tripton $\pi_a^+\pi^-\pi^0$ must fall in the ρ band, the tripton must be accompanied by a $\Delta^{++} \rightarrow p\pi_b^+$, and none of the constituents of the tripton are included in a Δ^{++} , ω^0 , or η^0 resonance.

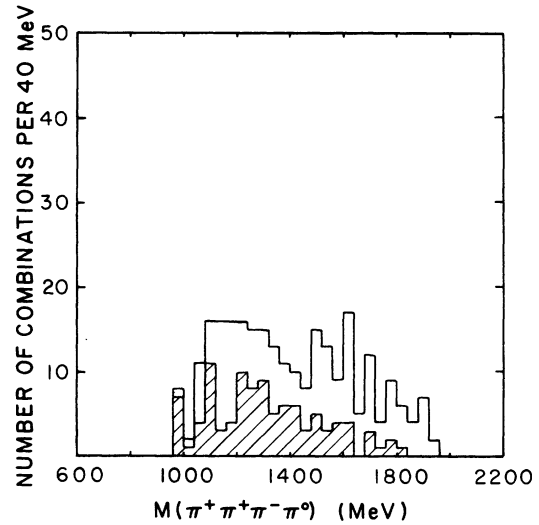


FIG. 6. Distributions in effective mass $M(\pi^+\pi^+\pi^-\pi^0)$ for reaction (1). Both histograms contain only those combinations for which neither π^+ is contained in a Δ^{++} resonance, and for which one $\pi^+\pi^-\pi^0$ combination lies in the ω^0 band. The clear histogram is for all values of $|t|$, the momentum transfer to the proton, while the shaded histogram contains events for which $|t| < 0.6$ (GeV/c)².

ratio for both η^0 and ω^0 production is sharply increased by limiting the distribution to events with small momentum transfer to the baryon. An indication of this is shown in the solid histogram of Fig. 4, which includes only those $\Delta^{++}\omega^0$ events in which the Δ^{++} is produced with a momentum transfer of $|t| < 0.6$ (GeV/c)². Both ω^0 and η^0 production practically disappear for $|t| > 1.0$ (GeV/

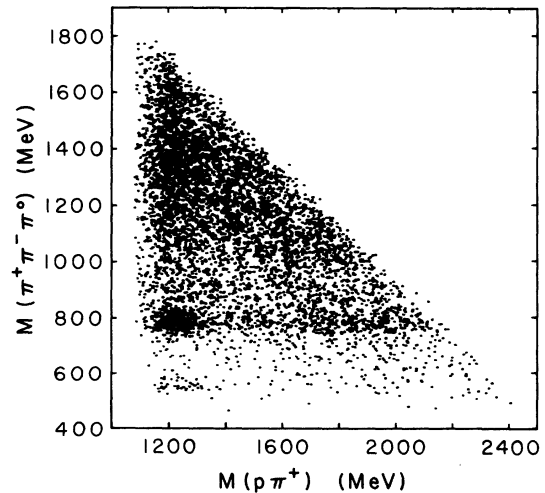


FIG. 7. Scatter plot for reaction (1), $M(\pi^+\pi^-\pi^0)$ vs $M(p\pi^+)$, two combinations per event.

TABLE IV. Cross sections for some quasi-two-body intermediate states of reaction (1).

Reaction ^a	Cross section at $p_{lab}=4.09$ GeV/c (this experiment)	Other experiments at nearby momenta	
		Cross section (mb)	p_{lab} (GeV/c)
(6) $\pi^+p \rightarrow \Delta^{++}\omega^0$	0.36 \pm 0.03	0.35 \pm 0.04	4.0 ^b
		0.39 \pm 0.04	4.08 ^c
(7) $\pi^+p \rightarrow \Delta^{++}\eta^0$	0.044 \pm 0.007	0.03 \pm 0.004	4.0 ^b
		0.043 \pm 0.008	4.08 ^c

^a The cross sections given here are for these reactions proceeding to the final state $p\pi^+\pi^+\pi^-\pi^0$.

^b M. Aderholz *et al.* (ABBLHM), Phys. Rev. **138**, B897 (1965).

^c Brown *et al.*, Ref. 2.

c)². Reaction (6) is discussed in detail in Sec. IV.

In the mass distribution of all the $\pi^+\pi^-\pi^0$ mass combinations (the clear histogram of Fig. 4), there is some indication of a signal in the A_2 region. The requirement that the $\pi^+\pi^-\pi^0$ combination be accompanied by a Δ^{++} (the shaded histogram of Fig. 4) enhances the signal in the mass interval $1240 < M(\pi^+\pi^-\pi^0) < 1440$ MeV/c², and reveals a small bump in the mass distribution in the A_1 region. The solid histogram which contains events with small momentum transfer [< 0.6 (GeV/c)²] to the Δ^{++} shows no such signals.

The distribution in $M(\pi_a^+\pi_b^-\pi^0)$, with $p\pi_b^+$ required to form a $\Delta^{++}(1236)$, has been replotted in Fig. 5 with the added requirement that one of the dipion combinations, $\pi_a^+\pi_b^-$, or $\pi_a^+\pi^0$, or $\pi_b^-\pi^0$, form a ρ resonance. This plot shows no further enhancement in the A -meson signal.

Four-pion mass combinations $M(\pi^+\pi^+\pi^-\pi^0)$ have been plotted, with the requirements that one of the $\pi^+\pi^-\pi^0$ combinations lie in the ω^0 band, and that the π^+ mesons are not shared with a Δ^{++} . In the clear histogram of Fig. 6 the distribution is plotted for all values of $|t|$, the momentum transfer to the proton, while in the shaded histogram only events with $|t| < 0.6$ (GeV/c)² are shown. There is no well-resolved B meson distinguishable in these histograms.

IV. THE INTERACTION $\pi^+p \rightarrow \Delta^{++}\omega^0 \rightarrow p\pi^+\pi^-\pi^0$

Of the quasi-two-body interactions observed, the one most amenable to analysis is

$$\pi^+p \rightarrow \Delta^{++}\omega^0 \quad (6)$$

because it occurs with reasonable frequency, and because the relatively small background can be

reduced to negligible proportions by limiting the study to events with low momentum transfer, thus effectively providing a pure sample. This reaction, represented in the diagram of Fig. 8, can proceed via ρ or B exchange, while π , f , η , and ω exchanges are forbidden.

Figure 9 contains a plot of $d\sigma/dt$ vs t for reaction (6). The data exhibit a dip in cross section for $|t| < \sim 0.15$ (GeV/c)², below a broad peak centered at $|t| \sim 0.2$ (GeV/c)², as expected for a reaction that proceeds mainly by vector-meson exchange. In the region $0.2 < |t| < 1.0$ (GeV/c)², the cross-section data are very well fitted by a single exponential: $d\sigma/dt = \text{const} \times e^{-b|t|}$. Values of b found by fitting an exponential to the data for various ranges of $|t|$ are given in Table V. Also given there for comparison are values of b obtained in other experiments at several different beam momenta. In the momentum transfer interval $0.2 < |t| < 1.0$ (GeV/c)², the data are consistent with a constant value of the exponent b ($b = 3.2 \pm 0.5$, 95% confidence level) for p_{lab} , the momentum of the incoming pion, ranging from 4.0 GeV/c to 18.5 GeV/c.

The data have been compared with the predictions of several models. The one-meson-exchange (OME) model without absorption is known not to give agreement with experimental results, except for reactions in which a pion may be exchanged. However, if absorption effects are in-

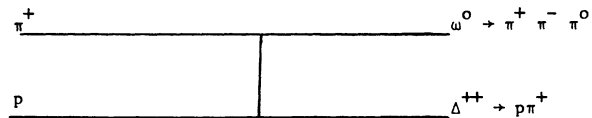


FIG. 8. Diagram for reaction (6).

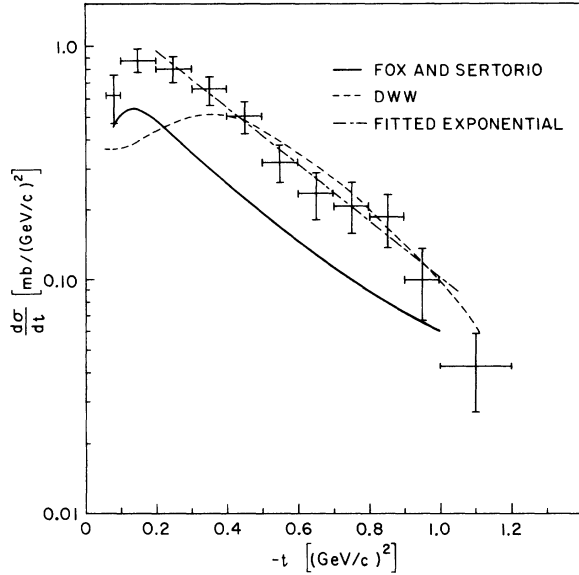


FIG. 9. $d\sigma/dt$ vs $-t$ for reaction (6). The dashed curve was calculated by Dar, Watts, and Weisskopf, Ref. 8; the full curve was found by interpolation from the calculations of Fox and Sertorio, Ref. 9. The dot-dash line is an exponential, fitted to the data over the interval $0.2 < |t| < 1.0$ (GeV/c)².

TABLE V. Values of b from fits of the experimental data to $d\sigma/dt = ae^{-b|t|}$, for the reaction $\pi^+p \rightarrow \Delta^{++}\omega^0$.

Momentum of incident pion (GeV/c)	Range of $ t $ (GeV/c) ²	b (GeV/c) ⁻²
4.0 ^{a,b}	$0.2 < t < 0.45$	3.83 ± 0.81
	$0.2 < t < 0.60$	2.28 ± 0.48
	$0.2 < t < 1.05$	2.67 ± 0.32
4.08 ^c	$0.2 < t < 1.2$	2.71 ± 0.28
	$0.2 < t < 0.44$	3.13 ± 0.51
4.09 (this experiment)	$0.2 < t < 0.60$	2.84 ± 0.28
	$0.2 < t < 1.00$	2.81 ± 0.15
	$0.15 < t' < 0.4^e$	4.4 ± 1.0
5.0 ^d	$0.15 < t' < 0.6$	3.7 ± 0.5
	$0.15 < t' < 1.0$	4.3 ± 0.3
	$ t' < 1.0^e$	2.67 ± 0.95
5.72 ^f	$0.15 < t' < 0.4^e$	3.2 ± 1.7
	$0.15 < t' < 0.6$	3.9 ± 0.7
8.0 ^g	$0.15 < t' < 1.0$	4.6 ± 0.5
	$0.1 < t' < 1.0^e$	3.6 ± 0.8

^aM. Aderholz *et al.*, Nuovo Cimento **35**, 659 (1965).

^bExponent factor b not given in the reference cited, but determined from data in the reference.

^cBrown *et al.*, Ref. 2.

^dPols *et al.*, Ref. 2.

^e $t' = t - t_{\min}$, where t_{\min} is the kinematic lower limit on momentum transfer, determined for each event. No substantial difference in exponents is found for our data when t' is used in place of t . A dip in $d\sigma/dt$ is still apparent for $|t'| < \sim 0.2$ (GeV/c)².

^fDao, Ref. 2.

^gM. Aderholz *et al.*, Nucl. Phys. **B8**, 45 (1968).

^hBiswas *et al.*, Ref. 2.

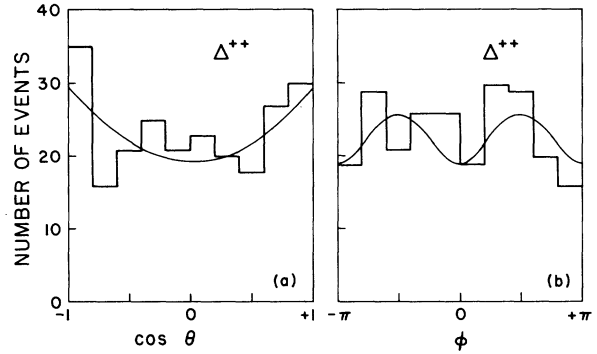


FIG. 10. (a) Gottfried-Jackson angle θ for Δ^{++} from reaction (6). θ is the angle between the incoming proton and the outgoing proton, in the rest frame of the Δ^{++} . (b) Treiman-Yang angle ϕ for Δ^{++} from reaction (6). ϕ is the azimuthal angle, with $\phi = 0^\circ$ in the production plane. The solid lines in (a) and (b) were found by making least-squares fits of Eqs. (9) to the data. Only events with $|t| < 0.6$ (GeV/c)² are included.

cluded, reasonably good agreement between model predictions and experiment can be obtained.⁷ The dashed line shown in Fig. 9 is calculated from the OMEA (one-meson exchange with absorption) model as modified by Dar, Watts, and Weisskopf (DWW),⁸ assuming ρ exchange.

For a Regge model, the absence of a dip in $d\sigma/dt$ at $|t| \approx 0.6$ (GeV/c)² indicates that ρ exchange alone is unsatisfactory. The solid line in Fig. 9 is the result of the Regge calculation of Fox and Sertorio,⁹ taking into account ρ and B primary and secondary (ρ' , B') trajectories. The last-mentioned curve for 4.09-GeV/c pions was

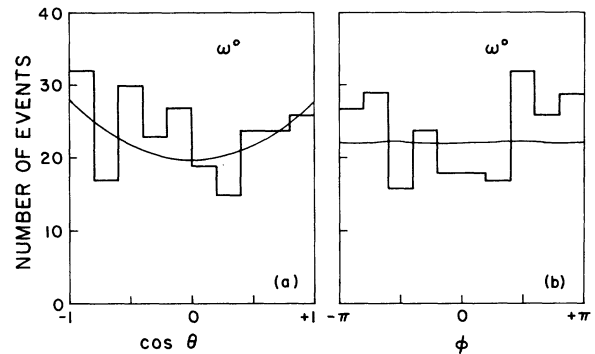


FIG. 11. (a) Gottfried-Jackson angle θ for ω^0 from reaction (6). θ is the angle between the incoming pion and the normal to the ω^0 decay plane in the ω^0 rest system. (b) Treiman-Yang angle ϕ , the azimuthal angle, which is equal to zero in the production plane. The solid lines in (a) and (b) were found by making least-squares fits of Eqs. (10) to the data. Only events with $|t| < 0.6$ (GeV/c)² are included.

obtained by interpolation from the Fox and Sertorio $d\sigma/dt$ vs t calculations for 3.5- and 5.0-GeV/ c pions. The interpolation was carried out under the assumption that the momentum dependence of the total cross section for reaction (6), $\sigma \propto p_{\text{lab}}^{-2.06}$,¹⁰ holds also for $d\sigma/dt$ at every t . The Fox and Sertorio curves for various values of p_{lab} appear to be in reasonable agreement with this assumption, especially for $|t| > 0.3$ (GeV/ c)², and the resulting curve for $p_{\text{lab}} = 4.09$ GeV/ c is insensitive to the details of the interpolation, except at $|t| < 0.3$ (GeV/ c)². A conservative upper limit for the calculated curve in the region $|t| < 0.3$ (GeV/ c)² can be established by the fact that the peak value of $d\sigma/dt$ obtainable from the Fox and Sertorio model for $p_{\text{lab}} = 4.09$ GeV/ c must be less than the value given by the model for $p_{\text{lab}} = 3.5$ GeV/ c , which is $d\sigma/dt = 0.7$ mb/(GeV/ c)² at $|t| = 0.14$ (GeV/ c)².

Both the DWW and the Fox-Sertorio curves agree with the data better than the OMEA-model calculations of Gottfried and Jackson⁷ which gave much too slow a decrease in $d\sigma/dt$ with increasing $|t|$. While the Fox and Sertorio Regge-model curve is low throughout the range of $|t|$ covered, its shape appears to conform better to the overall distribution of the data than the DWW curve. In Ref. 9 Fox and Sertorio give comparisons with data which show the calculations somewhat on the high side at $p_{\text{lab}} = 8.0$ GeV/ c , somewhat on the low side at 5.0 GeV/ c , and definitely low at 3.5 GeV/ c .

The spin-density-matrix elements ρ_{33} , ρ_{3-1} , and

ρ_{31} for the Δ^{++} , and ρ_{00} , ρ_{1-1} , and ρ_{10} for the ω^0 , have been determined from the experimental decay angular distributions by using the formulas given below.

For Δ^{++}

$$\begin{aligned} \frac{d\sigma}{d(\cos\theta)} &\propto 1 + 4\rho_{33} + (3 - 12\rho_{33}) \cos^2\theta, \\ \frac{d\sigma}{d\phi} &\propto 1 + (4/\sqrt{3}) \text{Re}(\rho_{3-1}) \\ &\quad - (8/\sqrt{3}) \text{Re}(\rho_{3-1}) \cos^2\phi, \\ \text{Re}(\rho_{31}) &= (5\sqrt{3}/8) \langle \sin 2\theta \cos\phi \rangle, \end{aligned} \quad (9)$$

where θ is the angle between the incoming proton and the outgoing proton, in the Δ^{++} cm system, and ϕ is the corresponding azimuthal angle, with $\phi = 0^\circ$ in the production plane (the Treiman-Yang angle).

For ω^0

$$\begin{aligned} \frac{d\sigma}{d(\cos\theta)} &\propto 1 - \rho_{00} + 3(\rho_{00} - 1) \cos^2\theta, \\ \frac{d\sigma}{d\phi} &\propto 1 + 2\rho_{1-1} - 4\rho_{1-1} \cos^2\phi, \\ \text{Re}(\rho_{10}) &= -(5/4\sqrt{2}) \langle \sin 2\theta \cos\phi \rangle, \end{aligned} \quad (10)$$

where θ is the angle between the incoming π and the normal to the ω decay plane in the ω rest system, and ϕ is the corresponding azimuthal angle, with $\phi = 0^\circ$ in the production plane. Figures 10 and 11 show the distributions in θ and ϕ for the Δ^{++} and ω^0 , respectively, for events of reaction

TABLE VI. Comparison of ρ_{ik} for interaction (6), determined in experiments at several laboratory momenta.

Momentum of incoming pion (GeV/ c)	Range of $ t $ used in fit (GeV/ c) ²	ω		Δ^{++}			
		ρ_{00}	ρ_{1-1}	$\text{Re}\rho_{10}$	ρ_{33}	$\text{Re}\rho_{3-1}$	$\text{Re}\rho_{31}$
4.09 (this experiment)	$ t < 0.6$	0.413 ± 0.056	0.003 ± 0.062	-0.122 ± 0.029	0.177 ± 0.037	0.068 ± 0.022	0.045 ± 0.034
4.0 ^a	$ t < 0.6$	0.47 ± 0.05	0.126 ± 0.045	-0.103 ± 0.026	0.15 ± 0.04	0.035 ± 0.040	-0.048 ± 0.038
3.92 ^b	$ t < 0.6$	0.48 ± 0.06	-0.04 ± 0.05	-0.14 ± 0.04	0.19 ± 0.04	0.02 ± 0.04	-0.07 ± 0.04
5.72 ^c	$ t < 0.6$	0.369 ± 0.081	0.037 ± 0.069	-0.069 ± 0.050	0.162 ± 0.061	0.069 ± 0.055	0.136 ± 0.057
18.5 ^d	$ t < 0.5$	0.26 ± 0.10	0.07 ± 0.09	0.05 ± 0.07	0.22 ± 0.08	-0.01 ± 0.08	-0.04 ± 0.08
Theoretical estimates							
4.0 ^e		0.46	0.13	-0.10	0.15	0.087	≈ 0
4.0 ^{f,g}					~ 0.1	~ 0.1	~ -0.05
5.0 ^{h,g}		~ 0.35	~ 0.09	~ -0.12	~ 0.23	~ 0.01	~ 0.03
8.0 ^{f,g}		~ 0.35	~ 0.15	~ 0.1	~ 0.2	~ 0.15	~ 0.02
8.0 ^e		0.31	0.24	-0.07	0.22	0.127	≈ 0

^aM. Aderholz *et al.*, Nuovo Cimento **35**, 659 (1965).

^bWinkelmann, Ref. 2.

^cDao, Ref. 2.

^dBiswas *et al.*, Ref. 2.

^eA. B. Kaidalov and B. M. Karnakov, Zh. Eksp. Teor. Fiz. Pis'ma, Red. **5**, 344 (1967) [JETP Lett. **5**, 284 (1967)].

^fDar, Watts, and Weisskopf, Ref. 8.

^gEstimates of average ρ_{ik} were made by us from ρ_{ik} vs t curves given in the reference.

^hFox and Sertorio, Ref. 9.

(6), with the limitation $|t| < 0.6 \text{ (GeV/c)}^2$ imposed to ensure a reasonably pure sample. The solid curves are least-squares fits of Eqs. (9) and (10) to the data. Table VI shows the average spin-density matrix elements determined from these data, and corresponding results from other experiments at various incident pion momenta, together with values predicted by several models. With a few exceptions, the average values of ρ_{ik} at the several momenta are consistent with each other, within the considerable errors. This result, and the apparent constancy of the exponent factor b over the incoming pion momentum range 4.0 to 18.5 GeV/c, support the assumption that the production mechanism remains the same throughout this momentum interval. The results of the model calculations are roughly consistent with the data.

A more sensitive test of a model should be given by studying the variation with t of the elements ρ_{ik} . Figures 12 and 13 show plots of these data for the ρ_{ik} of Δ^{++} and ω^0 , respectively; the solid curves are those of the Dar-Watts-Weisskopf mod-

el,⁸ and the dashed curves are from Fox and Sertorio for 5.0-GeV/c incident pions.⁹ Many more data are needed to refine the comparison. Although agreement is rather poor in some cases, it is not possible to rule out either model on the basis of these comparisons, given the large statistical uncertainties in the data now available.

The quantity $\rho_{00} d\sigma/dt$ is plotted in Fig. 14. This quantity contains contributions from 1^+ poles only, since 1^- particles do not couple to the $|00\rangle$ state of the $|\pi\omega\rangle$ vertex. This figure thus indicates the exchange of B -like poles in reaction (6). The decrease in $\rho_{00} d\sigma/dt$ for $|t| < 0.2 \text{ (GeV/c)}^2$, in agreement with the observation of Abrams *et al.*,¹¹ is much sharper than the decrease in $d\sigma/dt$ in this region (Fig. 9), and may arise from a change in polarization of the ω^0 in this region of $|t|$.

Density matrix elements depend on the reference system chosen, and Donahue and Högaasen (DH)¹²

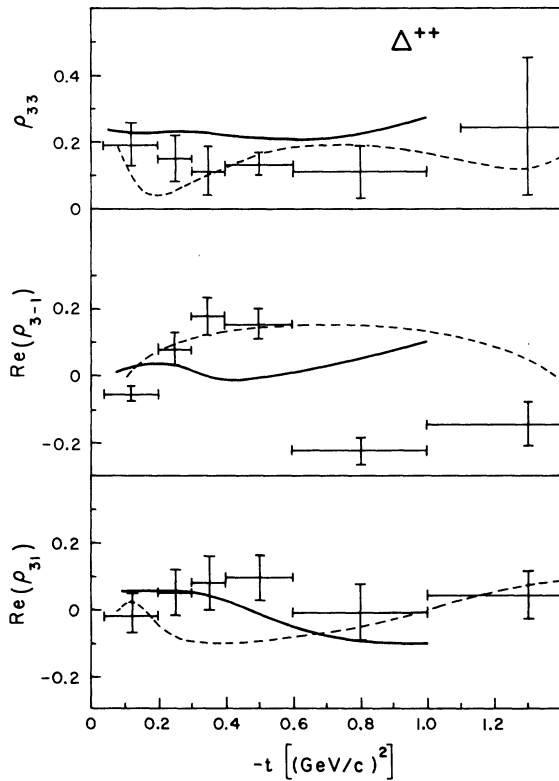


FIG. 12. ρ_{33} , $\text{Re}(\rho_{3-1})$, and $\text{Re}(\rho_{31})$ vs $-t$ for Δ^{++} (1236) from reaction (6). The curves are calculated: The dashed lines are from Ref. 8, for 4.0-GeV/c incident pions; the solid lines are from Ref. 9, for 5.0-GeV/c incident pions.

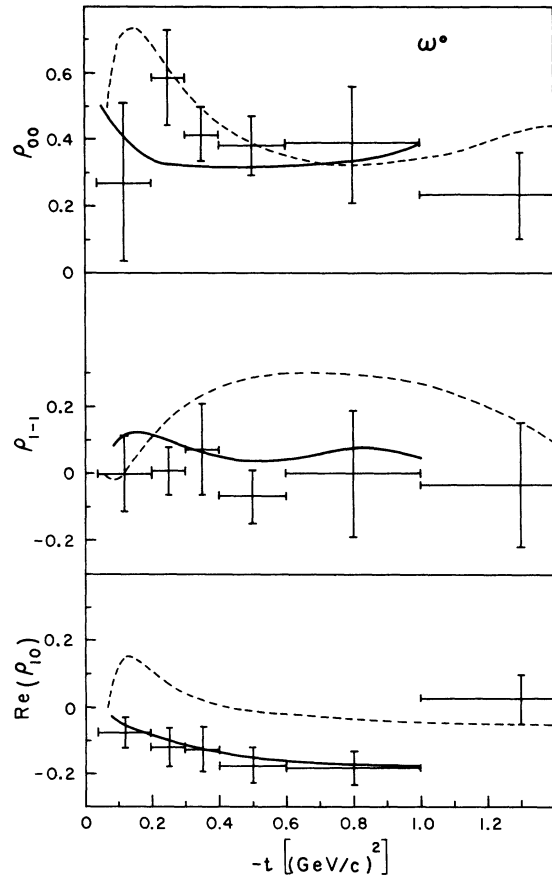


FIG. 13. ρ_{00} , ρ_{1-1} , and $\text{Re}(\rho_{10})$ vs $-t$ for ω^0 from reaction (6). The curves are calculated: The dashed lines are from Ref. 8, for 4.0-GeV/c incident pions; the solid lines are from Ref. 9, for 5.0-GeV/c incident pions.

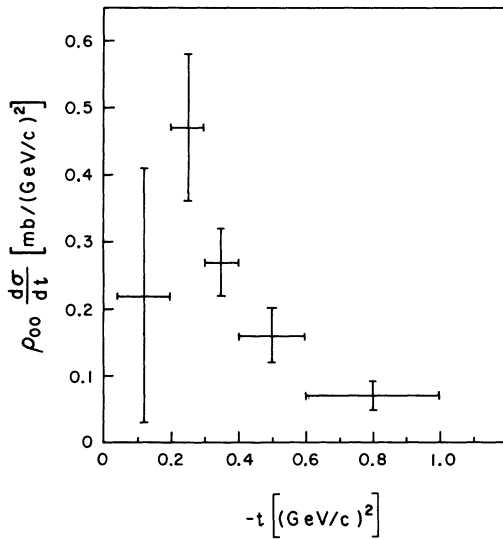


FIG. 14. The quantity $\rho_{00} d\sigma/dt$ vs $-t$ for reaction (6).

have suggested looking for a unique system in which the density matrix is reduced to its simplest possible general form. They suggest that such a system may be found by allowing a rotation around

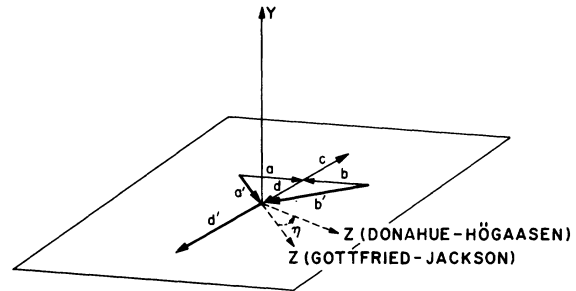
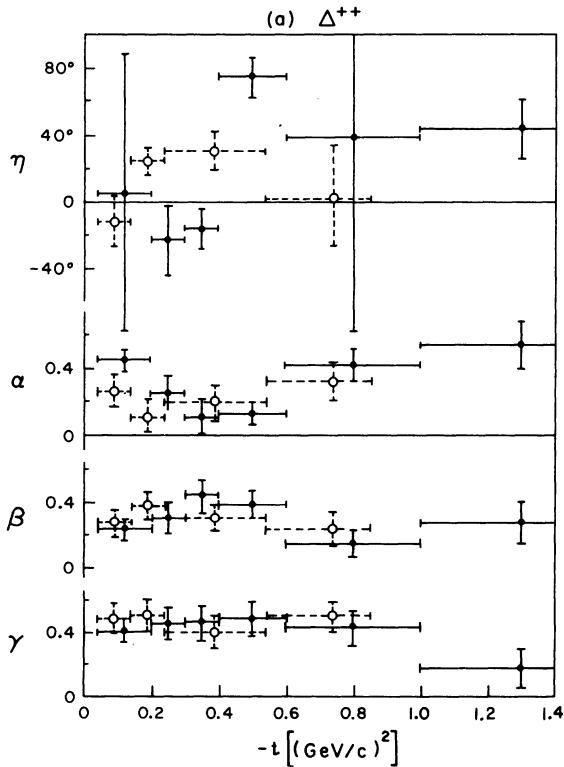


FIG. 15. Illustration of the relation between the Jackson (J) and the Donahue-Högaasen (DH) systems. The vector momenta of the particles in the reaction $a + b \rightarrow c + d$ are shown, c being the resonance of interest. The unprimed vectors are in the over-all center-of-mass system; the primed vectors are in the rest system of c . The J and DH systems have their y axes in common—the normal to the production plane, defined by the vector momenta of particles a , b , and d . The Jackson z axis is parallel to the direction of the momentum of the incident particle, a , as seen in the rest frame of c . The J and DH z axes are transformed into one another by a rotation η about y .

the normal to the production plane, from the Jackson z axis to the DH z axis, to a system for which the spin operator I_z is diagonal. In this new system the independent parameters ρ_{ik} are

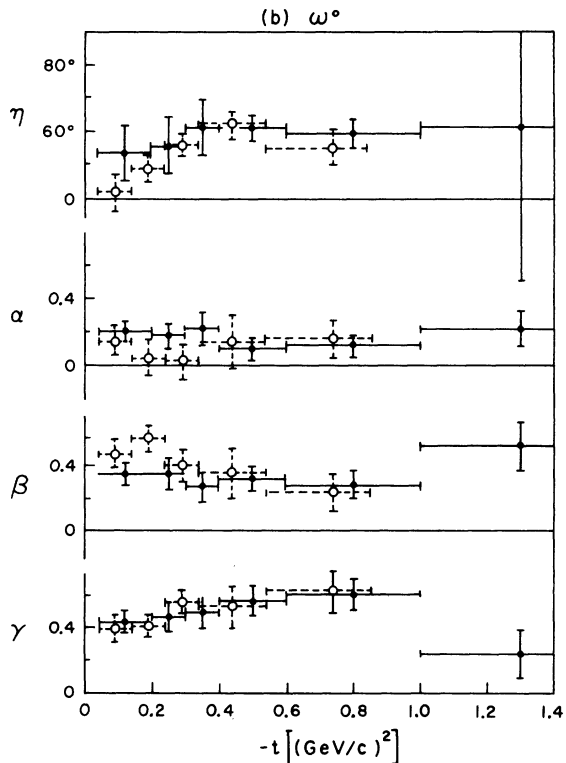


FIG. 16. Donahue-Högaasen parameters for reaction (6): (a) α , β , γ , and η for Δ^{++} ; (b) α , β , γ , and η for ω^0 . The points with solid error bars are the results of this experiment; the circles are the combined 4.0-GeV/c and 8.0-GeV/c data points from Ref. 16.

replaced by three non-negative eigenvalues, the diagonal matrix elements α , β , and γ , and the rotation angle η . Figure 15 illustrates the relation between the Jackson (J) and the DH systems.

Some evidence for the fundamental nature of density matrix elements in the DH system has been presented,¹³⁻¹⁶ and in Ref. 16 an experimental determination has been made of the Donahue-Högaasen spin population parameters, for 4.0-GeV/c pion-induced reactions. A brief description of the procedure and a determination of these parameters for the data of this experiment are presented here.

Donahue and Högaasen have given the following formula for the decay angular distribution in the DH system:

$$W(\hat{n}) = \frac{3}{4\pi} [\alpha \cos^2(\hat{n}, \hat{x}) + \beta \cos^2(\hat{n}, \hat{y}) + \gamma \cos^2(\hat{n}, \hat{z})], \quad (11)$$

with $\alpha + \beta + \gamma = 1$. The vector \hat{n} is a unit vector in the direction of one of the two decay particles of the Δ^{++} , or along the normal to the decay plane of the ω^0 . \hat{x} , \hat{y} , and \hat{z} are unit vectors along the DH axes.

To compute the DH parameters, $W(\hat{n})$ of Eq. (11) can be written in the form

$$W(\hat{n}) = \frac{3}{4\pi} [\alpha (\sin\theta \cos\phi \cos\eta - \cos\theta \sin\eta)^2 + \beta (\sin\theta \sin\phi)^2 + \gamma (\cos\theta \cos\eta + \sin\theta \cos\phi \sin\eta)^2], \quad (12)$$

where θ and ϕ are the Gottfried-Jackson and Treiman-Yang angles, and η is the angle of rotation between the Jackson and DH z axes. A three-parameter maximum-likelihood fit has been made to Eq. (12) to determine α , γ , and η . Since $\alpha + \beta + \gamma = 1$, β is thus determined also.

The experimentally determined values of the DH parameters as a function of t are plotted in Fig. 16. No effort has been made to correct for background, which is quite small for $|t| < 0.6$ (GeV/c)². Shown in Fig. 16 also are the 4.0- and 8.0-GeV/c experimental results of Aderholz *et al.*¹⁶ α , β , and γ are found to have much less variation with t than ρ_{ik} ; it is possible to infer from this, as Aderholz *et al.* do, that at least part of the variation with t of the matrix elements in the Jackson system is a kinematic effect, arising from the rotation η out of the "natural" DH frame. The residual variation with t of the DH parameters then can be taken to be a consequence of t -dependent mixtures of different exchanges.

It is of interest to see whether the data indicate evidence of correlations between the ω and Δ decays, as discussed by Barnham *et al.*¹⁷ These

authors, using the formulations of Pilkuhn and Svensson¹⁸ and of Donahue,¹⁹ have evaluated joint decay density matrices, in addition to the single vertex matrices described above. Although the statistics of this experiment do not warrant such a detailed analysis as was made in Ref. 17, evidence of correlations can be observed by plotting the decay angular distributions of the Δ separately for events in different intervals of $\cos\theta_\omega$, and similarly plotting the decay angular distributions of the ω separately for events in different intervals of $\cos\theta_\Delta$. Figures 17(a) and 17(b) show the distributions in $\cos\theta_\Delta$ for $|\cos\theta_\omega| < 0.4$ and $|\cos\theta_\omega| > 0.4$, respectively, while Figs. 17(c) and 17(d) show the distributions in $\cos\theta_\omega$ for $|\cos\theta_\Delta| < 0.4$ and $|\cos\theta_\Delta| > 0.4$, respectively. The solid curves are from Barnham *et al.*,¹⁷ and were calculated from their data, using their fitted single vertex and correlation terms. The differences between (a) and (b), for polar and equatorial ω decays, and between (c) and (d), for polar and equatorial Δ decays, are indications of the correlations between the decays. Agreement of the calculated curves from Ref. 17 with the data of the present experiment is very good.

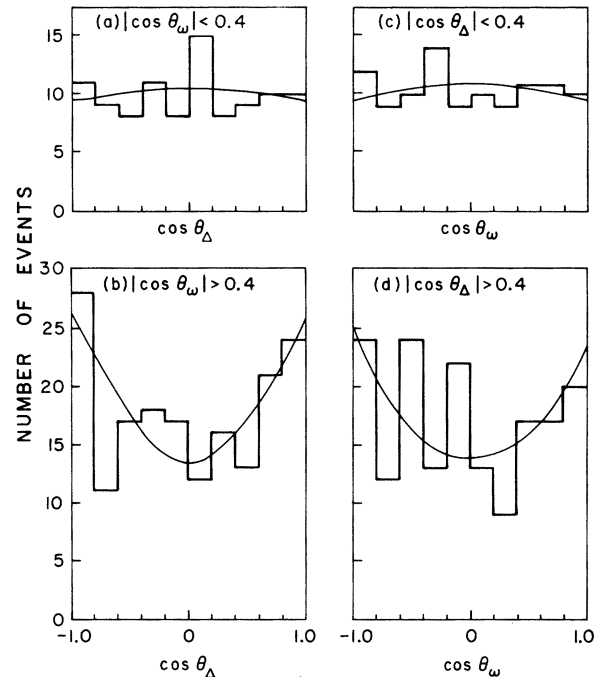


FIG. 17. (a) and (b) Distributions in $\cos\theta_\Delta$ for the two regions, $|\cos\theta_\omega| < 0.4$ and $|\cos\theta_\omega| > 0.4$, respectively. (c) and (d) Distributions in $\cos\theta_\omega$ for the two regions $|\cos\theta_\Delta| < 0.4$ and $|\cos\theta_\Delta| > 0.4$, respectively. The curves are those calculated by Barnham *et al.*, Ref. 17, from their fitted single-vertex and joint decay density matrix elements, and have been normalized to equal total numbers of events in the histogram in each plot.

ACKNOWLEDGMENTS

We wish to thank K. Kang and C.-I Tan for helpful discussions, and R. Reasenberg for his participation in the early stages of this experiment. We are happy to express our appreciation to L. Voyvodic, R. Walker, and the crews of the 30-in.

bubble chamber and of the ZGS at the Argonne National Laboratory for their aid in obtaining the film. We thank I. A. Pless and the staff of the MIT PEPR system for their unfailing cooperation, and we gratefully acknowledge the painstaking work of our scanning and measuring technicians.

*Work supported in part by the U. S. Atomic Energy Commission under Contract No. AT(11-1)-3130TB.

†Present address: Physics Department, Carleton University, Ottawa, Ontario, Canada.

¹Preliminary results have been presented at various meetings: S. Pitluck *et al.*, *Bull. Am. Phys. Soc.* 15, 493 (1970); 15, 537 (1970); D. G. Fong *et al.*, *ibid.* 16, 38 (1971).

²M. Aderholz *et al.*, *Phys. Rev.* 138, B897 (1965); *Nuovo Cimento* 35, 659 (1965); *Nucl. Phys.* B8, 45 (1968); D. Brown *et al.*, *Phys. Rev. D* 1, 3053 (1970); I. A. Pless *et al.*, in *Proceedings of the Fourteenth International Conference on High Energy Physics, Vienna, 1968*, edited by J. Prentki and J. Steinberger (CERN, Geneva, Switzerland, 1968); C. L. Pols *et al.*, *Nucl. Phys.* B25, 109 (1971); N. N. Biswas *et al.*, *Phys. Rev. D* 2, 2529 (1970); F. C. Winkelmann, Ph.D. thesis, MIT, 1968 (unpublished); F. T. Dao, Ph.D. thesis, MIT, 1970 (unpublished).

³S. Pitluck, Ph.D. thesis, Brown University, 1971 (unpublished).

⁴A. Citron *et al.*, *Phys. Rev. Lett.* 13, 205 (1964).

⁵D. G. Fong, A. M. Shapiro, and M. Widgoff, *Phys. Rev. D* 8, 3765 (1973).

⁶J. Bartsch *et al.*, *Nuovo Cimento* 43A, 1010 (1966).

⁷K. Gottfried and J. D. Jackson, *Nuovo Cimento* 33, 309 (1964); 34, 735 (1965); J. D. Jackson, *Rev. Mod. Phys.* 37, 484 (1965).

⁸A. Dar, T. L. Watts, and V. F. Weisskopf, *Nucl. Phys.* B13, 477 (1969).

⁹G. C. Fox and L. Sertorio, *Phys. Rev.* 176, 1739 (1968).

¹⁰E. Bracci *et al.*, CERN Report No. CERN/HERA 72-1, 1972 (unpublished).

¹¹G. S. Abrams *et al.*, *Phys. Rev. Lett.* 25, 617 (1970).

¹²J. T. Donahue and H. Høgaasen, *Phys. Lett.* 25B, 554 (1967).

¹³A. Białas and K. Zalewski, *Phys. Lett.* 28B, 436 (1969).

¹⁴M. Aderholz *et al.*, *Nucl. Phys.* B8, 485 (1968).

¹⁵W. De Baere *et al.*, *Nuovo Cimento* 61, 397 (1969).

¹⁶M. Aderholz *et al.*, *Nucl. Phys.* B24, 509 (1970).

¹⁷K. W. J. Barnham *et al.*, *Phys. Rev. D* 7, 1384 (1973).

¹⁸H. Pilkuhn and B. E. Y. Svensson, *Nuovo Cimento* 38, 518 (1965).

¹⁹J. T. Donahue, *Nuovo Cimento* 52A, 1152 (1967).